in turn are packed into a very compact helical aggregate, with much less space for molecular dynamics refinement to move the atoms within the particle. The energy barriers caused by the close contacts are so high that increasing the starting temperature without allowing thermal expansion of the particle would not be expected to overcome them.

In summary, molecular dynamics refinement against fiber diffraction has been shown to be an effective means of structure determination. Even when the initial structure is too far from the true structure to allow direct refinement, the method is able to find local minima that resemble the true structure sufficiently to allow improved phasing and thus lead to interpretable difference maps.

We thank Axel Brünger, Lee Makowski and Rekha Pattanayek for valuable discussions. This work was supported by NSF grants DIR-8915800 and DIR-9011014.

References

ARNOTT, S. & WONACOTT, A. J. (1966). *Polymer*, **7**, 157-166.
BERENDSEN, H. J. C., POSTMA, J. P. M., VAN GUNSTEREN, W. F., DINOLA, A. & HAAK, J. R. (1984). *J. Chem. Phys.* **81**, 3684-3690.
BROOKS, B. R., BRUCCOLERI, R. E., OLAFSON, B. D., STATES, D. J., SWAMINATHAN, S. & KARPLUS, M. (1983). *J. Comput. Chem.* **4**, 187-217.
BRÜNGER, A. T. (1990). *X-PLOR Manual.* Version 2.1. Yale Univ., New Haven, USA.
BRÜNGER, A. T., KARPLUS, M. & PETSKO, G. A. (1989). *Acta Cryst.* A**45**, 50-61.
BRÜNGER, A. T., KRUKOWSKI, A. & ERICKSON, J. (1990). *Acta Cryst.* A**46**, 585-593.
BRÜNGER, A. T., KURIYAN, J. & KARPLUS, M. (1987). *Science*, **235**, 458-460.
COCHRAN, W., CRICK, F. H. C. & VAND, V. (1952). *Acta Cryst.* **5**, 581-586.
FRANKLIN, R. E. & KLUG, A. (1955). *Acta Cryst.* **8**, 777-780.
GROS, P., FUJINAGA, M., DIJKSTRA, B. W., KALK, K. H. & HOL, W. G. J. (1989). *Acta Cryst.* B**45**, 488-499.
HENDRICKSON, W. A. (1985). *Methods in Enzymology*, Vol. 115, edited by H. W. WYCKOFF, C. H. W. HIRS & S. N. TIMASHEFF, pp. 252-270. Orlando: Academic Press.
KARPLUS, M. & PETSKO, G. A. (1990). *Nature (London)*, **347**, 631-639.
KLUG, A., CRICK, F. H. C. & WYCKOFF, H. W. (1958). *Acta Cryst.* **11**, 199-213.
MAKOWSKI, L. (1982). *J. Appl. Cryst.* **15**, 546-557.
MILLANE, R. P. (1989). *Acta Cryst.* A**45**, 573-576.
NAMBA, K., PATTANAYEK, R. & STUBBS, G. (1989). *J. Mol. Biol.* **208**, 307-325.
NAMBA, K. & STUBBS, G. (1985). *Acta Cryst.* A**41**, 252-262.
NAMBA, K. & STUBBS, G. (1987). *Acta Cryst.* A**43**, 533-539.
NAMBUDRIPAD, R. & MAKOWSKI, L. (1989). *Biophys. J.* **55**, 417*a*.
NAMPUDRIPAD, R. & MAKOWSKI, L. (1992). Unpublished results.
NAMBUDRIPAD, R., STARK, W. & MAKOWSKI, L. (1991). *J. Mol. Biol.* **220**, 349-379.
PATTANAYEK, R. & STUBBS, G. (1992). *J. Mol. Biol.* **228**, 516-528.
SMITH, P. J. C. & ARNOTT, S. (1978). *Acta Cryst.* A**34**, 3-11.
STUBBS, G. (1989). *Acta Cryst.* A**45**, 254-258.
STUBBS, G. & DIAMOND, R. (1975). *Acta Cryst.* A**31**, 709-718.
STUBBS, G. & MAKOWSKI, L. (1982). *Acta Cryst.* A**38**, 417-425.
STUBBS, G., NAMBA, K. & MAKOWSKI, L. (1986). *Biophys. J.* **49**, 58-60.
WANG, H., PATTANAYEK, R. & STUBBS, G. (1992). Unpublished results.
WASER, J. (1955). *Acta Cryst.* **8**, 142-150.

Acta Cryst. (1993). A**49**, 513-527

The Electron Distribution in Corundum. A Study of the Utility of Merging Single-Crystal and Powder Diffraction Data

BY ANTHONY S. BROWN AND MARK A. SPACKMAN

Department of Chemistry, University of New England, Armidale, NSW 2351, *Australia*

AND RODERICK J. HILL

CSIRO Division of Mineral Products, PO Box 124, *Port Melbourne, Victoria* 3207, *Australia*

(*Received* 22 *April* 1992; *accepted* 22 *October* 1992)

Abstract

Powder X-ray diffraction data for corundum were collected by a variety of methods and reduced to structure amplitudes by two profile-fitting techniques. The resulting averaged powder-data set was merged with three different single-crystal data sets to assess the improvements possible over least-squares modelling of extinction for accurate electron density analysis of minerals. With reference to the deformation electron density derived from multipole refinements, it is concluded that this strategy offers advantages over the *post facto* modelling of severe extinction effects commonly observed in such

0108-7673/93/030513-15$06.00

systems. The deformation electron density is found to be in quantitative agreement with the results of recent *ab initio* calculations on clusters and the bulk.

Introduction

As technologies and techniques for the measurement of accurate structure factors continue to improve, the potential for electron density analysis of the data to extract useful and chemically interesting information increases. However, this potential can only be realized if the effects of extinction can be eliminated or at least successfully modelled. While there are many cases where extinction is not a major problem, owing to the nature of the crystals involved, minerals can present serious extinction problems. Extinction is particularly problematic in accurate electron density studies, since it is the strong low-angle reflections that contribute most of the information on the bonding electron density; precisely those worst affected by extinction. Inadequate or inappropriate extinction corrections will therefore compromise the results of an electron density analysis. In preliminary work on stishovite, for example, Spackman, Hill & Gibbs (1987) noted that attempts to correct for extinction in several severely affected low-angle reflections with an extinction model resulted in regions of negative total electron density as derived from a multipole model. Schwarzenbach & Lewis (1982) and Coppens (1982) have described how anisotropic extinction corrections applied to corundum data can mimic electron density features near the nuclei and as a consequence may destroy information on the property under investigation, in that particular case, the electric-field gradients at the nuclei.

The best strategy to obtain a set of accurate structure factors suitable for detailed electron density analysis is obviously to choose samples and experimental conditions very carefully to eliminate, or at least to reduce to acceptably low levels, the effects of extinction. Small crystals and shorter-wavelength radiation, for example, may significantly reduce extinction but it may not be possible to remove the effect completely. Many minerals, in particular, exhibit severe extinction effects owing to the high degree of crystal perfection common in such systems (Spackman & Weber, 1988). It is generally believed that extinction corrections of the order of 5–10% on $|F_o|$ are reliably modelled by current extinction theories (Becker, 1977; Spackman & Weber, 1988) but for larger extinctions the situation is less clear.

If extinction cannot be reduced to relatively low levels by a favourable selection of sample and experimental conditions during single-crystal X-ray data collection, more suitable data may be obtained using electron or γ-ray diffraction. Alternatively, the method that will be examined in this study is the replacement of the worst extinction-affected structure factors from the single-crystal data with those determined from a powder diffraction experiment. Extinction effects are generally less pronounced in powder than in single-crystal diffraction (owing to the much smaller crystallite sizes in the powder sample; typically submicrometre) and the former may therefore yield more reliable estimates for the stronger low-angle reflections. Spackman *et al.* (1987) have reported an electron density analysis of stishovite based on a merged data set of this kind. With careful collection and reduction of both powder and single-crystal data sets and due attention to the merging procedure, they obtained a merged data set with extinction effects small enough to be modelled reliably with existing extinction formalisms. The analysis of the resulting data set was more successful than when severe extinction effects in the original single-crystal data set were modelled, and this conclusion has been recently supported by the good agreement between model deformation electron densities resulting from the merged data and the results of linearized plane-wave calculations (Cohen, 1991). There were, of course, new problems to be overcome in the merging procedure, such as the effects of preferred orientation in the powder sample, but it is possible that with care this approach may offer improvements over the application of extinction corrections to severely affected data sets.

Table 1. *Crystal data for corundum,* α-Al_2O_3

Space group	$R\bar{3}c$
Unit cell	$a = b = 4.760$, $c = 12.993$ Å
	$V = 255.0$ Å^3
	$Z = 6$
Number of reflections to $160°2\theta$ (Cu $K\alpha$)	67 (α_1 only)
Linear absorption coefficient (Cu $K\alpha$)	126.5 cm^{-1}

Corundum is an ideal candidate for a detailed study of this kind as there are several extensive single-crystal data sets already published and the electron density analyses of these are in significant disagreement. Relevant crystal data for corundum are provided in Table 1. The crystal structure can be described as a near-ideal hexagonal close packing of O atoms in which the Al atoms occupy two-thirds of the octahedral interstices. The AlO_6 octahedra that result from this arrangement form face-sharing pairs along the crystallographic c axis.

The present work has two related objectives. The first is to assess the utility of merging powder and single-crystal diffraction data sets as a means of overcoming some of the problems in electron density analysis that are associated with extinction. The second objective is the further investigation of the deformation electron density in corundum by electron density analysis of the diffraction data and its comparison with the results of recent *ab initio* theoretical cluster calculations (Brown & Spackman, 1992). A study of electric-field gradients emerging from the same analyses is the subject of a separate work.

Powder-data collection

Most commercially available powder diffractometers employ the Bragg–Brentano (BB) flat-plate sample parafocusing geometry for data acquisition (Jenkins, 1989). Hill & Madsen (1991) have recently reported modifications to a conventional BB parafocusing diffractometer that allows data to be collected in a Debye–Scherrer (DS) configuration using a capillary sample. They examined the characteristics of data collected with both BB and DS geometries. Both configurations have advantages and disadvantages that can be more or less important depending upon the use for which the data are collected (Hill & Madsen, 1991). In terms of collecting data suitable for use in accurate charge-density analyses, the main advantages of BB (reflection) geometry are that the diffracted intensities are relatively higher, the resolution is generally superior (*i.e.* reduced overlap between reflections) and absorption in the sample can be neglected since it is constant over the full range of 2θ. The main disadvantage of BB geometry is that the crystallites that make up the sample are prone to preferred orientation, though this can generally be reduced or eliminated by careful sample preparation. The major advantage of the DS geometry is that the effects of preferred orientation of crystallites in the sample can be greatly reduced by spinning the sample capillary about the 2θ axis. This advantage must, however, be weighed against the disadvantages of lower diffraction intensity, somewhat poorer resolution and the fact that the data are collected in transmission mode with the result that sample absorption is not constant and must be correctly modelled.

Five data sets were collected for this study using samples of chemically pure Buehler C corundum (mean particle size 1 μm) and a standard Philips PW1050 goniometer fitted with a PW1710 diffractometer controller system: four were collected with the conventional BB parafocusing configuration and one with the DS geometry as described by Hill & Madsen (1991). The data collection was carried out as described in detail in that work. Both instruments were operated with conventional Soller, divergence and receiving slits in place. The 1° divergence and receiving-slit dimensions used in the BB configuration were chosen on the basis of previous studies by Madsen & Hill (1988) and represent a compromise between resolution and intensity. For the DS configuration, a 1° receiving slit and a 0.25° divergence slit were used, the dimensions of the divergence slit being the minimum that allowed the sample capillary to be completely bathed in the incident beam. All data sets were collected using Cu $K\alpha$ radiation, monochromatization being achieved with a nickel β filter for the BB configuration and a diffracted-beam curved graphite monochromator for the DS configuration. The use of Cu $K\alpha$ radiation represents an effective compromise between the increase in peak overlap resulting from use of a shorter-wavelength radiation (such as Mo $K\alpha$) and the reduced number of accessible reflections obtained with a longer wavelength (such as Co $K\alpha$). Data were collected at step intervals of $0.025°2\theta$ over the range $20–160°2\theta$ with step counting times of 10 s. The sample in the BB configuration is contained in the rectangular window of a standard aluminium sample holder. The sample used with the DS configuration was mounted in a Lindemann-glass capillary with a nominal internal diameter of 0.5 mm.

A number of different techniques were used to load samples into the sample containers in an effort to gauge the effects of different sample-preparation methods on the diffraction pattern. This was of particular interest for the data sets collected in the BB geometry, since the flat stationary sample is more prone to the effects of preferred orientation (if present) than the cylindrical rotated sample in the DS geometry. The sample used for the DS data collection was simply drifted into the glass capillaries. For the samples used for BB data collection, three sample-loading regimes were used. The first was the standard method of back-pressing the sample into the rectangular window of the aluminium sample holder. This method gives possibly the greatest risk of preferred orientation since the crystallites are compacted together. The second method involves back-pressing the sample into the sample holder as before, followed by scraping the surface to remove the more oriented 'skin' caused by surface compaction. The final method of sample loading was to side-drift the sample into the holder. This technique is intended to reduce the risk of inducing preferred orientation, since the particles are allowed to settle gently into place and are not compacted, thus (hopefully) allowing a more random orientation of each particle.

Both Rietveld (1969) and non-structure-based (Pawley, 1981; Will, 1989) profile-fitting procedures were used to extract integrated peak intensities from the step-scanned diffraction patterns. Rietveld refinements were performed with the program *RIET7*, a development of programs by Wiles & Young (1981) and Hill & Howard (1986), and peak-fitting refinements were performed with the program *PROFIT* (Scott, 1987).

Rietveld refinements using both neutral-atom and ionic scattering-factor models were carried out for each data set using strategies described by Hill (1984) and Hill & Madsen (1991). Scattering factors for Al, O and Al^{3+} and anomalous-dispersion corrections for Al and O atoms were taken from *International Tables for X-ray Crystallography* (1974) and the scattering factor for O^{2-} from Hovestreydt (1983). The refinements for the data collected with the DS geometry were performed with a version of the *RIET7* program that explicitly corrects for the absorption in

a cylindrical sample, which, in the DS geometry, is a function of 2θ. This absorption correction is based on the known packing density of the sample and interpolations of μr values tabulated by Weber (1967). Initially, all refinements included the background fitted as a four-parameter polynomial in 2θ. It was found that for the DS data the background could not be adequately modelled in this way owing to the presence of non-uniform scattering from the glass capillary. The DS data were therefore modelled using a background determined by interpolation between 18 points selected in the range 20–160°2θ. The peak-shape function used in the Rietveld refinements was the pseudo-Voigt, with the fraction of Lorentzian character varied as a function of 2θ. Release of a preferred-orientation parameter of the March type (Dollase, 1986) showed that this was a negligible feature in all data sets, most probably due to the small size of the crystallites in the sample. The agreement between the observed and calculated step intensities can be gauged with the Bragg R factor for powder refinements, $R_B = \sum_k |I_{o,k} - I_{c,k}| / \sum_k I_{o,k}$, where $I_{o,k}$ and $I_{c,k}$ are the observed and calculated intensities, respectively, for the kth peak. With this measure of agreement between the model and the observations, the refinements that used the ionic model yielded consistently better agreement with the observations ($R_B = 3$–4%) than the neutral-atom model ($R_B = 4$–5%).*

In the profile-fitting (also known as pattern-decomposition) procedure, the observed step intensities are fitted with a model in which the heights of resolvable Bragg peaks and their peak shapes are refined (rather than the crystal structure parameters, as in Rietveld analysis). The positions of the peaks are constrained by the known lattice parameters but a refinable polynomial allows for small adjustments in the lattice parameters. The peak-shape function used in all peak-fitting refinements was, as in the Rietveld refinements, the pseudo-Voigt function with the fraction of Lorentzian character varied as a function of 2θ. The background was modelled as a four-parameter polynomial in 2θ for the BB data sets and by interpolation between 18 points in the range 20–160°2θ for the DS data set. Plot output of the refinements of a typical BB data set and the DS data set are provided in Fig. 1. Indices of the major peaks have been added where appropriate.

Structure factors for each data set were obtained from the integrated peak intensities by application of the standard geometric factors. The structure amplitudes derived from the data collected with the DS geometry are somewhat problematic in the sense that the pattern has a lower signal-to-noise ratio, there is a greater degree of peak overlap and the background is less uniform than that obtained with BB geometry (see Fig. 1) and thus it could not be refined as a polynomial function of 2θ as noted previously. With an interpolation of the background in the DS data other problems arose, particularly the presence of two negative intensities for the very weak reflections 315 and $32\bar{2}$ (this problem arises because the selection of the points for interpolation is, of necessity, a subjective process). As a result of these difficulties, the DS data were excluded from consideration in the production of the final powder-data set.

An important difference between the Rietveld refinements with neutral-atom and ionic scattering factors and the peak-fitting refinements arises because of the way overlapping peaks are treated in the various procedures. The number of partially or completely overlapping peaks in the corundum powder patterns used in the present study is 27 for both the BB and DS data (out of a total of 67 unique reflections). In the Rietveld method, the intensity in a region where two or more peaks overlap is partitioned between the contributing peaks on the basis of the crystal-structure and scattering-factor model that is used. The choice of neutral-atom or ionic scattering factors can therefore lead to minor differences in the way overlapping peak intensities are partitioned. On the other hand, the profile-fitting (pattern-decomposition) procedure provides a more objective method of assigning intensities in this situation since it does not rely on an electron density model. In the present work, any possible difficulties associated with overlapping peaks were minimized by averaging the results of the three methods of partitioning overlapping peak intensities, which hopefully negates much of the bias that may be introduced by use of only one method of partitioning.

More complex structures that give rise to diffraction patterns with a higher proportion of strongly overlapping peaks are likely to provide even greater difficulties for the application of the present merging procedure because of the problems involved in the assignment of intensities to individual peaks. Indeed, there is considerable current activity in the search for more efficient and accurate methods of crystal-structure-independent peak deconvolution as increasing numbers of powder patterns are used to provide structure factors for *ab initio* crystal-structure solution (see, for example, McCusker, 1991; Gilmore, Henderson & Bricogne, 1991). These methods include maximum entropy (Bricogne, 1991) and the examination of triplet and quartet relationships (Jansen, Peschar & Schenk, 1990). The new techniques are especially relevant in certain space groups with large

* We note that the integrated peak intensities for overlapping reflections are not directly extracted from the powder pattern in a Rietveld analysis, so that there is no 'observed' peak intensity, as such. Instead, the 'observed' intensity is estimated for each reflection in an overlapping group by partitioning the full observed intensity at each step among the contributing reflections in accordance with their calculated step intensities. No such procedure is required for free-standing peaks in the pattern.

numbers of exact overlaps due to the symmetry constraints of the lattice (note that for corundum no reflections exactly overlap). In these cases, no advantage can be gained by the collection of higher-resolution data, say on a synchrotron X-ray source, since the reflections necessarily have the same d spacing. In fact, the highly parallel X-ray beams used in synchrotron experiments can produce additional problems for powder work owing to the difficulties that may then arise in achieving a 'powder average'.

Although standard deviations for the intensities determined by Rietveld or peak-fitting methods are available, there is some doubt as to their validity as true measures of the uncertainties of the intensities (Scott, 1988). The pragmatic approach taken in the present work is to average the best 12 sets of structure factors and use the standard deviation of the structure factors in each data set from the mean structure factor as the best available estimate of the uncertainty associated with each structure factor. This was the powder-data set used in subsequent merging with single-crystal data and is designated 'Cu:powd'.

Since an objective of this work is to assess the utility of merging powder and single-crystal data, emphasis has been placed upon the powder-data collection and extraction of structure amplitudes and their e.s.d.s. No attempt was made to collect single-crystal data as several such extensive data sets have previously been reported by Lewis, Schwarzenbach & Flack (1982) (referred to here as LSF) and by Kirfel

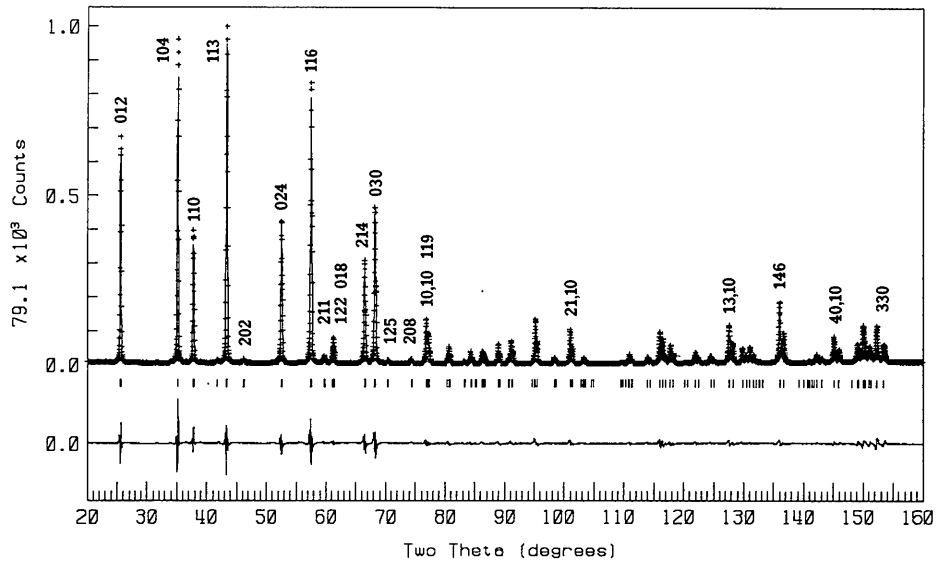

(*a*)

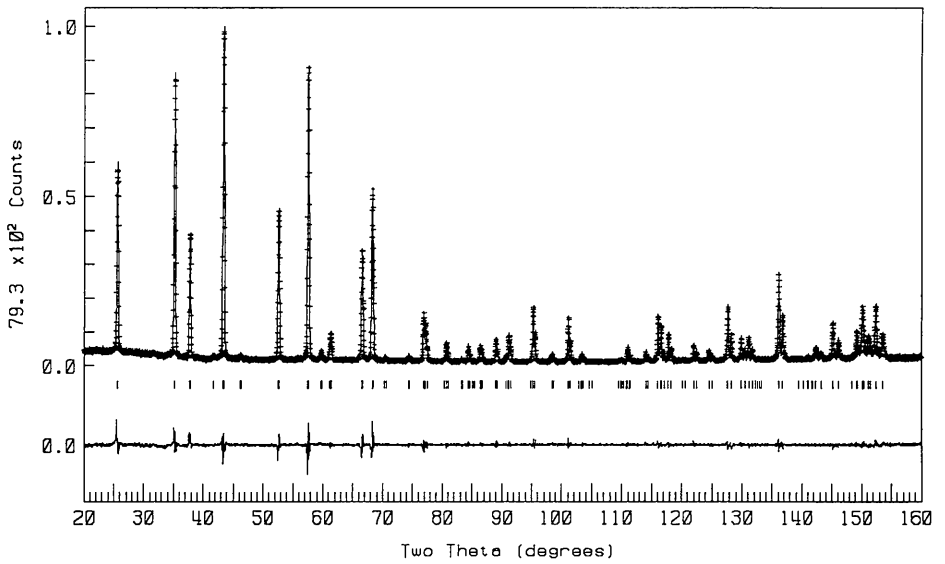

(*b*)

Fig. 1. Plot output from the profile-fitting refinements of (*a*) a typical Bragg-Brentano (BB) data set and (*b*) the Debye-Scherrer (DS) powder diffraction data set for corundum. In each plot, + represents the observed step-scan data points, the calculated profile is the continuous line overlaying them and the 'difference' curve is the lower profile. The positions of all possible reflections allowed by the space group are shown as the row of vertical tick marks. Indexing has been provided for certain reflections.

Table 2. *Details of the data sets used in the merging procedure*

The Ag:xtal and Mo:xtal data sets are from Lewis *et al.* (1982) and the SR:xtal data set is from Kirfel & Eichhorn (1990).

	Ag:xtal	Mo:xtal	SR:xtal	Cu:powd
Sample type	Single crystal	Single crystal	Single crystal	Powder
Radiation	Ag $K\alpha$	Mo $K\alpha$	Synchrotron	Cu $K\alpha$
λ(Å)	0.56083	0.71069	0.5599	1.5418
$(\sin\theta/\lambda)_{max}$ (Å^{-1})	1.495	1.19	1.024	0.639
Number of reflections	804	397	258	61
Maximum extinction correction (%)*	13	24	36	-

* As reported in the original references.

& Eichhorn (1990) (referred to here as KE). The relevant details of each original data set used in the present work are summarized in Table 2. 'Ag:xtal' and 'Mo:xtal' are the single-crystal data sets of LSF collected with Ag $K\alpha$ and Mo $K\alpha$ radiation, respectively. Ag:xtal displays moderate extinction, requiring a maximum extinction correction of 13%, and represents probably the best single-crystal data set currently available for corundum. Mo:xtal exhibits more severe extinction than Ag:xtal, having a maximum correction of 24%, and is therefore a suitable candidate for merging with powder data. 'SR:xtal' is the single-crystal data set of KE collected with synchrotron radiation ($\lambda = 0.56$ Å), which exhibits even more severe extinction than either Ag:xtal or Mo:xtal, with a maximum correction of 36%. However, the weak reflections in this data set were reported by KE as being measured more accurately than is possible with tube radiation. This data set is also a good candidate for merging. 'Cu:powd' is the averaged powder data set described in the previous section.*

Merging procedure

Spackman *et al.* (1987) have previously outlined the procedure used to merge powder and single-crystal data sets. What follows is a more detailed description of the technique as applied to the corundum data sets. Initially, the parameters of a conventional spherical-atom model were refined using only high-angle Ag:xtal data ($\sin\theta/\lambda \geq 0.80$ Å^{-1}) to yield the least-biased estimates of position and thermal parameters for Al and O in corundum. The scale and an isotropic-extinction parameter [type 1 model, Lorentzian mosaic (Becker & Coppens, 1974)] were also refined. Trial refinements of various isotropic extinction models (type 1 and type 2 models with Gaussian or Lorentzian mosaic) for each of the three single-crystal data sets confirmed the preference for the type 1 Lorentzian mosaic model (in agreement with LSF and KE). This extinction model was therefore adopted for all subsequent charge-density models. For the Cu:powd data set with a spherical-atom model and fixed high-angle position and thermal parameters, the isotropic-extinction parameter and scale were then refined so that these data were on a near-absolute scale prior to merging. The Cu:powd data exhibited no extinction effects based on this refinement.

The anomalous-dispersion contributions to Ag:xtal, Mo:xtal, SR:xtal and Cu:powd are significantly different and must be accounted for in the merging procedure, from the point of view of both the final scaling of the data sets and the subsequent refinement of charge-density models based on the merged data. For the merging of Mo:xtal and Cu:powd, the observed structure factors in the two experiments can be written as

$$F_o(\mathrm{Cu}) = A_o + A_s(\mathrm{Cu}) + i[B_o + B_s(\mathrm{Cu})] \quad (1)$$

and

$$F_o(\mathrm{Mo}) = A_o + A_s(\mathrm{Mo}) + i[B_o + B_s(\mathrm{Mo})], \quad (2)$$

where A_o and B_o are dispersion free and A_s(Cu), A_s(Mo), B_s(Cu) and B_s(Mo) are the anomalous-dispersion contributions for Cu $K\alpha$ and Mo $K\alpha$ radiations. A_s and B_s are insensitive to small changes in structural and thermal parameters (Spackman *et al.*, 1987). For the Cu:powd data they were determined from the spherical-atom refinement just described and for the single-crystal data sets from a preliminary multipole refinement. In all cases, the dispersion corrections were from *International Tables for X-ray Crystallography* (1974). Since corundum is centrosymmetric, B_o is zero for all reflections and (1) above can be solved for A_o,

$$A_o = -A_s(\mathrm{Cu}) \pm [|F_o(\mathrm{Cu})|^2 - |B_s(\mathrm{Cu})|^2]^{1/2}, \quad (3)$$

where the sign of A_o is given by the phase as determined from the refinement. A set of Mo-equivalent reflections can then be prepared by applying the Mo $K\alpha$ dispersion corrections,

$$|F'(\mathrm{Cu})| = [A_o^2 + 2A_oA_s(\mathrm{Mo}) + A_s(\mathrm{Mo})^2 + B_s(\mathrm{Mo})^2]^{1/2}, \quad (4)$$

where F'(Cu) represents an Mo $K\alpha$-equivalent powder reflection.

* A list of averaged structure factors derived from the Cu:powd data set has been deposited with the British Library Document Supply Centre as Supplementary Publication No. SUP55690 (2 pp.). Copies may be obtained through The Technical Editor, International Union of Crystallography, 5 Abbey Square, Chester CH1 2HU, England.

A scale factor was calculated to bring the powder- and single-crystal-data sets onto a common scale prior to the merge by minimization of δ given by

$$\delta = \sum w[k|F'(\mathrm{Cu})| - y^{-1}|F_o(\mathrm{Mo})|]^2, \quad (5)$$

where the weights are given by $w = 1/\sigma^2(F)_{\mathrm{powd}} + 1/\sigma^2(F)_{\mathrm{xtal}}$, k is the scale factor, $|F'(\mathrm{Cu})|$ and $|F_o(\mathrm{Mo})|$ are the Mo $K\alpha$-equivalent powder and Mo:xtal structure-factor magnitudes, respectively, and y is the extinction correction from the preliminary multipole refinement of Mo:xtal data (if extinction had been present in the powder data, this too could be included in the expression). For δ to be minimized, we must have

$$k = \sum wy^{-1}|F_o(\mathrm{Mo})||F'(\mathrm{Cu})|/\sum w|F'(\mathrm{Cu})|^2. \quad (6)$$

The procedure is analogous for merging Ag:xtal and SR:xtal with Cu:powd, with dispersion corrections appropriate to the wavelengths of the Ag $K\alpha$ and synchrotron radiations (the latter interpolated from known values) substituted for those of Mo $K\alpha$. Only those reflections for which the extinction correction to the single-crystal observation was less than 5% of $|F_o|$ (based on the preliminary multipole refinement) were used to calculate the scale factor.

'Ag:merge', 'Mo:merge' and 'SR:merge' data sets were prepared by respectively replacing 9, 18 and 25 single-crystal reflections in the Ag:xtal, Mo:xtal and SR:xtal data sets (those for which the extinction correction was greater than or equal to 5% of $|F_o|$, based on the preliminary multipole refinement) with the corresponding scaled and dispersion-corrected powder reflection. This is a somewhat arbitrary procedure but represents a (reasonable) conviction that, in the absence of severe extinction effects, the estimate of $|F_o|$ provided by the single-crystal data is more reliable and more precise than that afforded by the powder sample. In all subsequent refinements of the merged data sets, extinction corrections were applied only to the single-crystal reflections, the powder reflections being considered extinction free as discussed above. The absence of measurable extinction effects in the powder data is consistent with the very small mean crystallite size in the Buehler C corundum sample, estimated to be in the submicrometre region based on the small degree of size broadening witnessed in the powder diffraction peaks.

Data analysis

A detailed comparison was made of refinements emerging from three different single-crystal and three different merged data sets. The multipole-expansion model of Stewart (1973, 1976) was used extensively in initial analyses of the single-crystal data sets. However, this model proved to be insufficiently flexible to model the diffraction data adequately, when applied with only one radial function for each multipole term. This was most striking in the case of the Ag:xtal data, where it was found that most of the deformation density in the vicinity of the O atoms was in fact modelled by very diffuse hexadecapole functions centred on the Al atoms. The Al pseudoatoms that resulted from these refinements violated the 'locality principle' advocated by Kurki-Suonio (1977), whereby it is desirable that most of the electron density in the vicinity of a particular atom should be described by functions centred on that atom. It is noteworthy that this model was used by KE in their analysis of, and comparison between, the Ag:xtal and SR:xtal data sets. However, unlike KE, we did not allow all exponents for each multipole order to vary; this would have led to convergence difficulties (as discussed by KE) and to further problems with diffuse functions (not mentioned by KE).* The more flexible model due to Hirshfeld (1971, 1977), which has more than one radial function for each multipole order up to the quadrupole level, proved to be more successful in modelling the electron density in corundum. A further advantage is that the Hirshfeld formalism was used by LSF in their analyses, so a direct comparison with their results is possible.

The electron density model refinements were performed using the *VALRAY* programs (Stewart & Spackman, 1983). To avoid bias in the results due to differences in the extent of each merged data set, refinements were performed using only those reflections with $\sin\theta/\lambda \le 1.024$ Å^{-1} (the limit of the least-extensive single-crystal data set, SR:xtal), which allowed direct comparison of maps and model parameters. This restriction of the data sets reduces the number of reflections to 260. It should also be noted that the SR:xtal and SR:merge data sets contain only 258 reflections, as the data deposited by KE and used by them in their study is missing the 0,0,12 and $10\bar{8}$ reflections. Multipole refinements were carried out with reference to a Cartesian coordinate system with $x\|[100]$, $y\|[120]$ and $z\|[001]$.

The scattering factors for neutral spherical Al and O atoms were calculated from the Hartree–Fock atomic wave functions of Clementi (1965). All refinements included anomalous-dispersion corrections from *International Tables for X-ray Crystallography* (1974) and an isotropic extinction parameter g (type I, Lorentzian) in the Becker–Coppens formalism (Becker & Coppens, 1974). In the absence of mean path lengths for each reflection (symmetry-averaged data were used), a value of $\bar{t} = 0.3$ mm was assumed in all refinements. The parameters in the

* An initial attempt was made to reproduce the multipole refinement of synchrotron data (MUSY) described by KE. A virtually identical fit to the data was obtained, but the resulting deformation electron density differed from their Fig. 9(a), being more like the present Fig. 6(a). We cannot explain this discrepancy and discuss the matter further below.

model were in each case optimized by least-squares minimization of $\varepsilon = \sum w(|F_o|^2 - |F_c|^2)^2$, where $w = \sigma^{-2}(|F_o|^2)$ and $|F_o|$ and $|F_c|$ are the observed and calculated structure-factor magnitudes, respectively. The minimization procedure has been described in detail by Spackman & Stewart (1984); convergence to a local minimum was checked by inclusion of second derivatives in the final cycle of least-squares minimization and the criterion for convergence recommended in that work was satisfied for all refinements. The e.s.d.s reported here for model parameters and electrostatic properties were obtained from the complete inverse least-squares matrices including second derivatives; covariances between parameters are thus included in the calculation of the e.s.d.s.

Minor modifications to the *VALRAY* code enabled specification of a multipole model equivalent to that described by Hirshfeld (1971, 1977). These modifications allow $F(000)$ to be included as a 'slack constraint' in the refinement, which ensured a correct electron count. The aspherical pseudoatoms of this model were constructed from the multipole functions of Stewart (1973, 1976) and are described using the nomenclature outlined by Stewart and by Stewart & Spackman (1983). Owing to the high site symmetries of the Al and O atoms, the number of allowed multipole functions for each pseudoatom is reduced from the 35 listed by Hirshfeld (1977). For Al on a threefold axis at $(0, 0, z)$, the allowed multipoles are the three monopoles, two sets of dipoles (d_3), two sets of quadrupoles (q_5), one set of octopoles (o_1, o_2, o_7) and one set of hexadecapoles (h_3, h_4, h_9); for O on a twofold axis at $(x, 0, \frac{1}{4})$, there are the three monopoles, two sets of dipoles (d_1), two sets of quadrupoles (q_1, q_4, q_5), one set of octopoles (o_1, o_4, o_5) and one set of hexadecapoles (h_1, h_4, h_5, h_8, h_9). All the multipoles on Al share a common radial exponent, α_{Al}, and those on O share α_O. The populations and exponents of all the allowed multipoles on both pseudoatom types were refined, which along with isotropic extinction, position and thermal parameters yielded a total of 43 variables in the model.

The inclusion of $F(000)$ as a slack constraint implies that the scale of the data is reasonably well known. The application of the slack constraint in the present refinements and the determination of the scale factor for the Ag: xtal, Mo: xtal and SR: xtal data sets was somewhat laborious. The data sets from LSF and KE were initially assumed to be on an absolute scale, to within a few percent. This was confirmed by a conventional spherical-atom high-angle refinement of each data set. The best scale (in the least-squares sense) was then determined by the following method. A value for $F(000)$ was calculated that included the contributions due to anomalous dispersion and this was added to the list of observed structure factors with an (arbitrary) e.s.d. of 0.1%. The parameters of the Hirshfeld model described above were then refined. The value of $F(000)$ was then scaled slightly so that its new value was within 1% of the original value and the model was refined again. This procedure was repeated with different scale factors until a minimum in the sum of squares of residuals was obtained. The scale determined for the Ag: xtal and Mo: xtal data sets was entirely consistent with the scale determined by LSF in their multipole refinements. The scale for the SR: xtal data set was within 2% of that determined by KE. This difference is not unexpected, since the multipole model used by KE was similar to the one used initially in the present work (*i.e.* that of Stewart) but later found to be too inflexible to model the Ag: xtal and Mo: xtal data adequately. However, differences in scale of the order of 1 to 2% have a major effect on the deformation density maps only in the regions close to the nuclei, so an error of approximately 0.5 to 1% in the scale factor will have only a small effect on the deformation density maps.

Direct-space deformation electron density maps and residual Fourier maps were calculated in two planes of interest. Plane 1 is the (010) plane containing one O and two Al atoms plus an inversion centre, with two further O atoms 0.12 Å out of the plane. Plane 2 is the (001) plane passing through the three O atoms that form a shared octahedral face. The map dimensions are 4.8×8.0 and 4.8×4.8 Å, respectively.

Merging *versus* conventional extinction corrections

(*a*) *Refinement results*

Before a discussion of the refinement results emerging from the various data sets (Table 3), it is important to appreciate that it is difficult to compare refinement indices that derive from fits to subtly different data sets, subsets of which have statistically distinct e.s.d.s. With this in mind, the fit to the data appears to be improved for the merged Ag $K\alpha$ and Mo $K\alpha$ data but worsened for the synchrotron data; extinction parameters are uniformly, but not significantly, larger after merging (although this does not mean that the extinction correction is necessarily greater as it depends upon the electron density model). Marginal increases in some of the R factors for the merged data-set refinements relative to the unmerged data-set refinements are observed, even for cases where ε and goodness-of-fit indices are improved. It is also evident that the positional and thermal parameters obtained from the refinements of the merged data sets are within one e.s.d. of the values from the refinements of the corresponding single-crystal data sets.

The radial-function exponents on each atom are generally greater for refinements of the merged data sets, corresponding to a sharpening of the deformation functions. An exception is the Al atom in the

Table 3. *Position parameters* ($\times 10^5$), *anisotropic thermal parameters* ($Å^2 \times 10^5$), *radial exponents* (a.u.$^{-1}$), *extinction parameters* ($g \times 10^4$ rad^2) *and refinement statistics for Hirshfeld-model refinements with single-crystal and merged powder/single-crystal data sets*

For all refinements, $(\sin\theta/\lambda)_{max} = 1.024$ Å^{-1}. $\varepsilon = \sum w(|F_o|^2 - |F_c|^2)^2$; $R(|F|) = \sum |F_o - F_c| / \sum |F_o|$; $wR(|F|^2) = [\varepsilon / \sum w|F_o|^4]^{1/2}$; GoF = $[\varepsilon/(n_{obs} - n_{var})]^{1/2}$. No weak reflections were excluded from the refinements. n_{powd} is the number of power reflections in the merged data set.

		Ag:xtal	Ag:merge	Mo:xtal	Mo:merge	SR:xtal	SR:merge
Al	z	35219 (2)	35218 (2)	35212 (5)	36216 (3)	35221 (1)	35222 (2)
	U_{11}	282 (3)	276 (5)	254 (13)	262 (6)	257 (5)	253 (5)
	U_{33}	291 (5)	290 (6)	258 (26)	280 (15)	257 (9)	245 (12)
	α_{Al}	2.3 (1)	3.0 (2)	4.7 (9)	3.7 (6)	3.6 (4)	3.9 (3)
O	x	30616 (10)	30614 (10)	30631 (4)	30627 (7)	30626 (6)	30623 (5)
	U_{11}	339 (11)	342 (14)	318 (4)	318 (5)	301 (6)	299 (7)
	U_{22}	359 (11)	358 (13)	343 (6)	339 (6)	318 (6)	316 (6)
	U_{33}	359 (10)	361 (11)	361 (5)	357 (6)	339 (9)	328 (9)
	U_{23}	65 (9)	66 (10)	69 (4)	63 (6)	60 (4)	57 (5)
	α_O	3.1 (3)	3.6 (4)	2.1 (2)	3.0 (6)	3.7 (4)	3.7 (6)
	g	0.16 (1)	0.17 (1)	0.22 (1)	0.26 (1)	0.72 (2)	0.86 (5)
	ε	598.7	595.5	2256.5	2077.3	226.4	233.2
	GoF	1.66	1.65	3.22	3.09	1.02	1.04
	$R(F)$ (%)	1.06	1.10	0.85	0.87	0.71	0.85
	$wR(F^2)$ (%)	1.33	1.35	1.47	1.44	1.62	1.64
	n_{obs}	261	261	261	261	259	259
	n_{var}	43	43	43	43	43	43
	n_{powd}	0	9	0	18	0	25

Mo $K\alpha$ data sets, where the exponent of 4.7 (9) a.u.$^{-1}$ obtained with the Mo:xtal data set (a very sharp function for an Al atom) falls to 3.7 (6) a.u.$^{-1}$ in Mo:merge.

(*b*) *Deformation electron densities*

Deformation and residual electron densities in the two planes of interest are given in Figs. 2 to 7 for the six refinements summarized in Table 3. Fig. 2 shows the deformation and residual electron densities in plane 1 for the Ag:xtal and Ag:merge data set refinements. The main features in the deformation density are present in both the Ag:xtal and Ag:merge maps, namely an elongated lobe of positive deformation density associated with the O atom on the right of the map, three lobes of positive deformation density around the O atoms to the left of the map and deep troughs of negative deformation density at the Al sites. There are some differences of note, particularly the positive deformation density features on either side of the Al sites in the Ag:xtal map, which are absent from the Ag:merge map, and the fact that the positive features in the Ag:merge map are typically one contour (0.05 e Å^{-3}) smaller than the corresponding features in the Ag:xtal map. There is little to choose between the residual density maps, both showing features that do not appear to indicate systematic problems with the data or the model (with the possible exception of a 'chicken-wire' arrangement of positive features, some as large as 0.2 e Å^{-3}, which may suggest systematic errors in a small number of structure factors).

Fig. 3 shows the deformation and residual density maps in plane 2 for the same data sets as in Fig. 2. Again, the same deformation density features are present in both the Ag:xtal and Ag:merge maps, with the features in the latter map typically being one contour (0.05 e Å^{-3}) smaller than in the former. Both maps show three lobes of positive deformation density about each O atom, one directed towards the centre of the shared octahedral face and the remaining two directed away from the shared face. As for plane 1, the residual density maps show no features that indicate systematic problems with either the data sets or the models. This is consistent with the observation that the improvement in the fit to the data for Ag:merge compared with Ag:xtal is only marginal (ε decreases from 599 to 596 and the goodness of fit from 1.66 to 1.65).

The Ag:xtal data set, being the least extinction-affected data set, would be expected to show the least improvement when merged with powder data. Examination of the maps for the Mo $K\alpha$ data sets (Figs. 4 and 5), on the other hand, show definite improvements due to the merging procedure. The deformation density in plane 1 for the Mo:xtal data set shows some similarity with the corresponding map for the Ag:xtal data set, particularly around the O atoms. However, the elongated positive feature associated with the O atom on the right of the Ag:xtal map has been replaced in the Mo:xtal map by two resolved lobes separated by a saddle point. In addition, there are four lobes of positive deformation density quite close to the Al nuclei, two of which are oriented along **c** and have peak heights of 0.25 e Å^{-3}

and far greater than 0.5 e Å^{-3}, respectively. The residual density in this plane (Fig. 4*b*) gives further cause for concern as the map displays what appears to be bands of positive residual density running along **c**. The large residual density features near the Al nuclear sites are particularly noteworthy as they indicate that even the large positive lobes of deformation density at these sites (Fig. 4*a*) are unable to account fully for the observed structure factors. It is reasonable to expect that Fig. 4(*a*) should closely resemble that reported by Schwarzenbach & Lewis (1982, Fig. 3) from a Hirshfeld refinement of the full Mo:xtal data, set. There are, however, significant differences between the two maps, which we attribute to the use of different extinction models in the two refinements.

For the Mo data, the effect of the merging procedure on the residual density maps is dramatic, as might be expected from the improved fit to the data for the Mo:merge data set (ε dropped from 2256 to 2077 and the goodness of fit from 3.22 to 3.09). The residual density map for the Mo:merge data set (Fig. 4*d*) is much flatter and is largely free of the systematic features noted in the Mo:xtal residual density map (Fig. 4*b*). The deformation density map for the Mo:merge data (Fig. 4*c*) is in qualitative agreement with the corresponding Ag:merge map (Fig. 2*c*).

In plane 2 for the Mo:xtal data set (Fig. 5*a*), the O atoms of the shared octahedral face again show three lobes of deformation density but they are quite dissimilar to those obtained with the Ag $K\alpha$ data sets. There is only a small lobe directed towards the centre of the shared face and two quite large lobes directed away from the shared face that have peak maxima three times the size of the smaller lobe. In the Ag $K\alpha$ data sets, the peak maxima for the three lobes were almost identical. The residual density map again shows what appears to be a systematic problem, with residual density accumulations at the O nuclear sites and at sites related to them by an approximate sixfold rotation axis perpendicular to the centre of the shared face. The latter three sites are of particular concern as they are not nuclear sites where one might expect problems (with an incorrect scale factor, for example). The residual density map in plane 2 for Mo:merge (Fig. 5*b*) is a striking improvement over the corresponding Mo:xtal map. It is almost featureless and lacks the systematic problem evident in the Mo:xtal residual density map. The deformation density map in this plane (Fig. 5*c*) agrees closely with the corresponding Ag:merge map: the O atoms of the shared octahedral face now display three lobes of positive deformation density with almost identical peak heights, as observed for the Ag $K\alpha$ data sets.

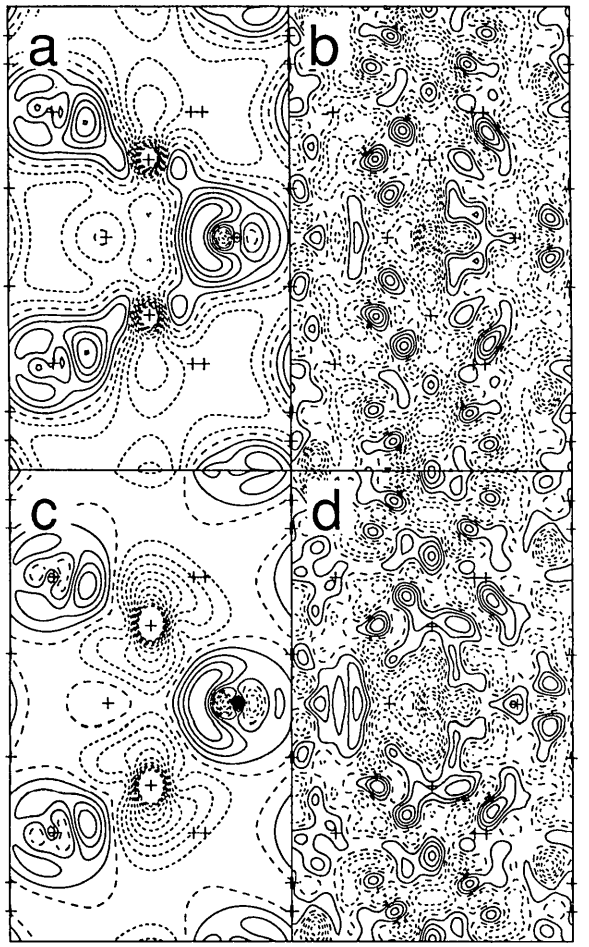

Fig. 2. (*a*), (*c*) Static multipole deformation density and (*b*), (*d*) residual Fourier maps in plane 1 obtained in multipole refinements with (*a*), (*b*) Ag:xtal and (*c*), (*d*) Ag:merge data sets. Contour interval 0.05 e Å^{-3}; $(\sin\theta/\lambda)_{max} = 1.024$ Å^{-1}.

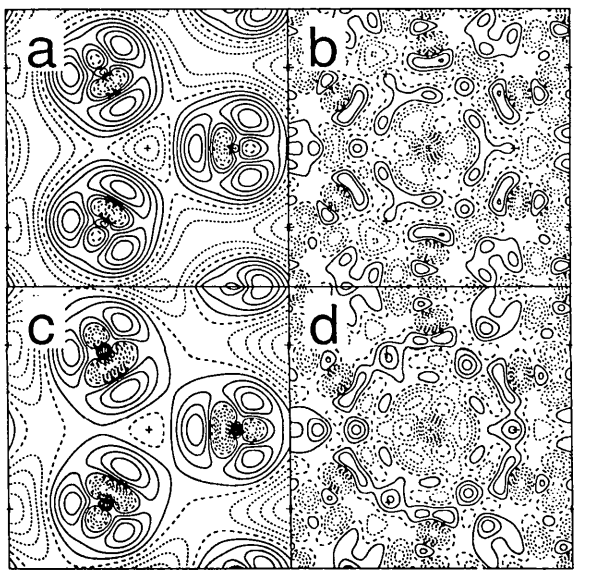

Fig. 3. (*a*), (*c*) Static multipole deformation density and (*b*), (*d*) residual Fourier maps in plane 2 obtained in multipole refinements with (*a*), (*b*) Ag:xtal and (*c*), (*d*) Ag:merge data sets. Contour interval 0.05 e Å^{-3}; $(\sin\theta/\lambda)_{max} = 1.024$ Å^{-1}.

In spite of a much higher level of extinction in the SR:xtal data (see Table 2), which requires a larger number of powder reflections (*viz* 25) to be merged, the fit to the merged data appears slightly worse than for the SR:xtal data, with ε increasing from 226 to 233 and the goodness of fit from 1.02 to 1.04. This is reflected in the residual density maps (Figs. 6 and 7). In plane 1, the SR:merge residual density maps display more positive residual density features than the SR:xtal map but they do not appear to be systematic features. In plane 2, the residual density map for the SR:xtal data set is very flat and clear of any major features. The corresponding map for the SR:merge data set displays significant positive residual density features in the shared octahedral face, with a peak at the centre of the map. The deformation density maps for the synchrotron data sets (Figs. 6*a*,*c* and 7*a*,*c*) display features that are markedly different from the maps obtained from conventional X-ray data. While the O atoms on the left of the maps (Fig. 6*a*,*c*) are surrounded by three lobes of positive deformation density and the Al sites coincide with deep troughs of negative deformation density as observed also in the Ag $K\alpha$ and Mo $K\alpha$ data sets, the features in the vicinity of the O atom at the right of the maps are significantly different. In the SR:xtal map (Fig. 6*a*), the O atom of the shared octahedral face is surrounded by four lobes of positive deformation density, two of which are localized along the Al–O bond vectors and the remaining two directed away from the shared face. After the merge, the latter two lobes are not resolved but form a single elongated ridge of deformation density. The deformation density maps in plane 2 (Figs. 7*a*,*c*) indicate that the O atoms of the shared octahedral face have only two lobes of positive deformation density that are directed away from the centre of the shared face. KE attributed the absence of positive deformation density in the shared octahedral face to the almost complete resolution of the deformation density into discrete lobes directed towards the adjacent Al atoms as previously described.

The map published by KE using the SR:xtal data for the deformation density in plane 1 [Fig. 9(*a*) in that work] shows some significant differences from that obtained in the present study. The O atom at the left of the KE map is surrounded by three lobes of positive deformation density, two of which are directed at ~90° to the O–Al bond vector and the third directed away from the Al atom. None of the lobes are directed toward the nearest-neighbour Al atom. There is also a relatively sharp dipolar deformation density feature (partly obscured in the original article)

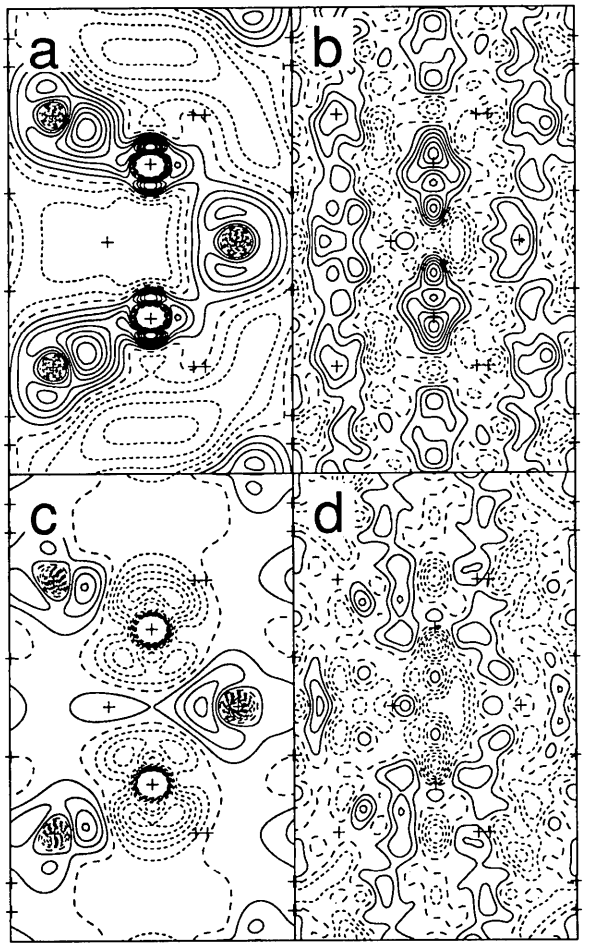

Fig. 4. (*a*), (*c*) Static multipole deformation density and (*b*), (*d*) residual Fourier maps in plane 1 obtained in multipole refinements with (*a*), (*b*) Mo:xtal and (*c*), (*d*) Mo:merge data sets. Contour interval 0.05 e Å^{-3}; $(\sin\theta/\lambda)_{max} = 1.024$ Å^{-1}.

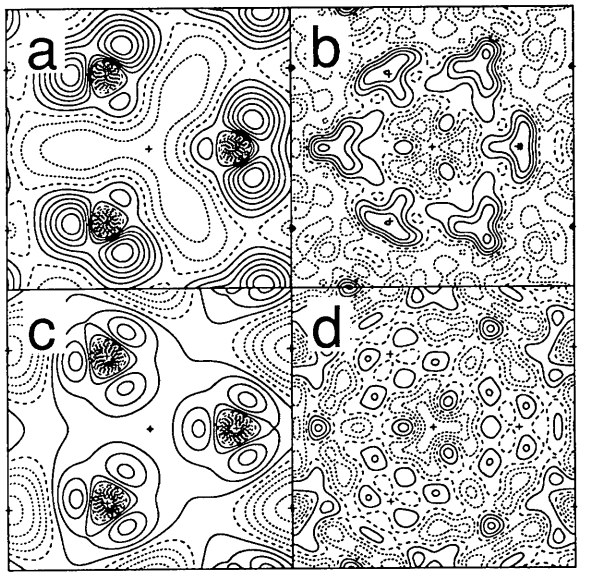

Fig. 5. (*a*), (*c*) Static multipole deformation density and (*b*), (*d*) residual Fourier maps in plane 2 obtained in multipole refinements with (*a*), (*b*) Mo:xtal and (*c*), (*d*) Mo:merge data sets. Contour interval 0.05 e Å^{-3}; $(\sin\theta/\lambda)_{max} = 1.024$ Å^{-1}.

close to the Al nuclear site. These features are absent from the maps in the present work, in the work of LSF and from the best theoretical calculations (Salasco, Dovesi, Orlando, Causa' & Saunders, 1991; Brown & Spackman, 1992). The origin of these seemingly anomalous features is not clear.

The presence of positive deformation density in the shared octahedral face in corundum has been consistently observed in previous experimental and theoretical studies. In their study of ruby ($Al_2O_3:Cr^{3+}$), Tsirelson, Antipin, Gerr, Ozerov & Struchkov (1985) reported deformation density features about the O atoms in question that agree with the features reported by LSF. Deformation density maps obtained *via* Fourier synthesis in the isostructural Ti_2O_3 and V_2O_3 also clearly display three lobes of electron density around the O atoms in the shared face, with heights between 0.15 and 0.25 e Å^{-3} (Vincent, Yvon, Grüttner & Ashkenazi, 1980; Vincent, Yvon & Ashkenazi, 1980). The presence of significant positive deformation density features in the shared face is also predicted by the various *ab initio* calculations by Dovesi and co-workers (Causa', Dovesi, Roetti, Kotomin & Saunders, 1987; Pisani, Causa', Dovesi & Roetti, 1987; Salasco *et al.*, 1991) and by Brown & Spackman (1992).

The collection of diffraction data suitable for accurate electron density analysis with use of synchrotron radiation is, by comparison with data collection using conventional X-ray sources, still very much in its infancy. The synchrotron data used in the present work was collected by KE in what they described as a 'feasibility study'. It would seem that, although the use of synchrotron radiation may lead to improved accuracy in the measurements of the weaker reflections, there remain as yet unidentified problems with this particular data set. Thus, it may perhaps be prudent to await further experience in the collection of synchrotron data for these purposes before embarkation on a detailed electron density analysis with such data.

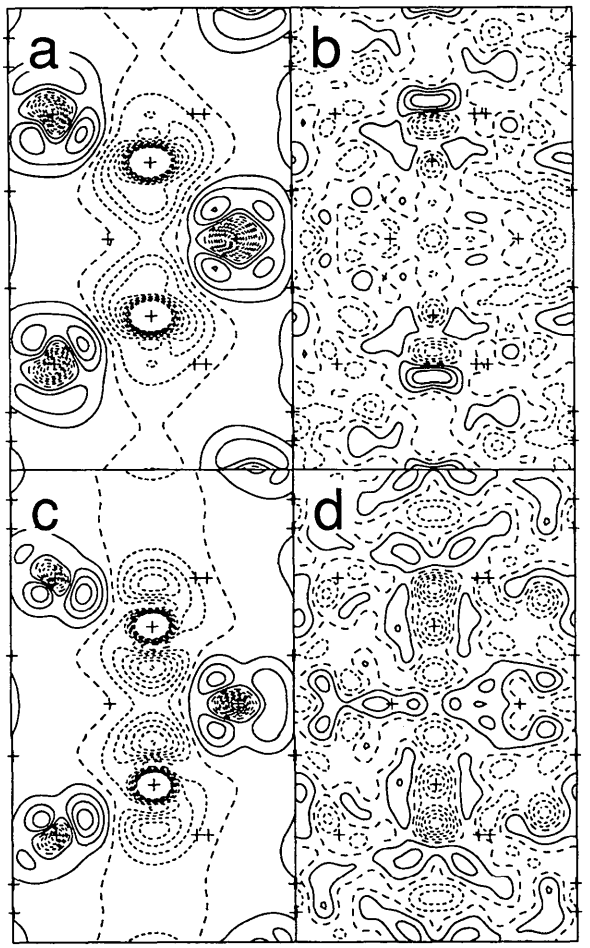

Fig. 6. (*a*), (*c*) Static multipole deformation density and (*b*), (*d*) residual Fourier maps in plane 1 obtained in multipole refinements with (*a*), (*b*) SR:xtal and (*c*), (*d*) SR:merge data sets. Contour interval 0.05 e Å^{-3}; $(\sin\theta/\lambda)_{max} = 1.024$ Å^{-1}.

Refinements with complete Ag:xtal and Ag:merge data sets

In the preceding section, it was shown that the merging procedure was successful as a means of reducing the effects of extinction in the conventional tube-source Ag $K\alpha$ and Mo $K\alpha$ data sets, as indicated by the improved fits of the pseudoatom models to the merged data. For the purposes of comparison with *ab initio* theoretical results, it is desirable that refinements of the pseudoatom models using the most

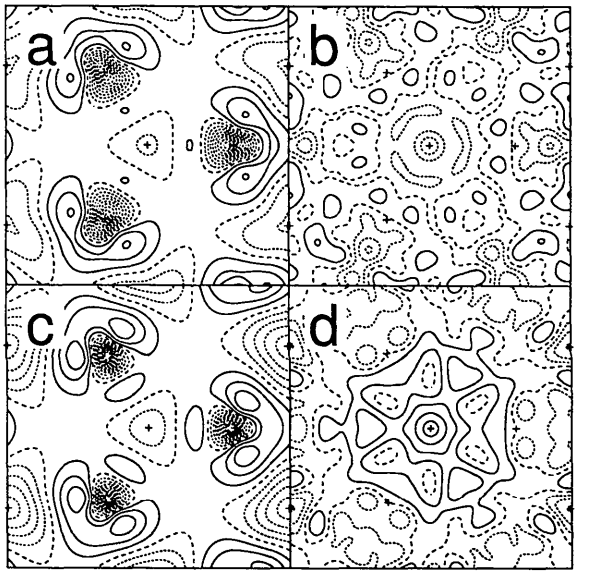

Fig. 7. (*a*), (*c*) Static multipole deformation density and (*b*), (*d*) residual Fourier maps in plane 2 obtained in multipole refinements with (*a*), (*b*) SR:xtal and (*c*), (*d*) SR:merge data sets. Contour interval 0.05 e Å^{-3}; $(\sin\theta/\lambda)_{max} = 1.024$ Å^{-1}.

Table 4. *Position parameters* ($\times 10^5$), *anisotropic thermal parameters* ($Å^2 \times 10^2$), *radial exponents* (a.u.$^{-1}$), *extinction parameters* ($g \times 10^4$ rad^2) *and refinement statistics for Hirshfeld-model refinements with Ag : xtal and Ag : merge data sets*

n_{powd} is the number of powder reflections in the data set.

		Ag : xtal	Ag : merge	Ag : xtal*
Al	z	35216 (1)	35215 (1)	35216 (1)
	U_{11}	279 (1)	277 (2)	279 (3)
	U_{33}	295 (2)	296 (2)	296 (3)
	α_{Al}	2.3 (1)	3.0 (2)	2.3 (1)
O	x	30624 (4)	30624 (5)	30624 (4)
	U_{11}	327 (3)	327 (3)	327 (3)
	U_{22}	346 (4)	345 (4)	341 (3)
	U_{33}	362 (4)	362 (4)	365 (3)
	U_{23}	60 (3)	60 (3)	Not given
	α_O	3.0 (2)	3.4 (2)	3.7 (1)
	g	0.15 (1)	0.17 (1)	-
	ε	1202.5	1190.2	-
	GoF	1.26	1.25	-
	$R(F)$ (%)	2.59	2.60	-
	$wR(F^2)$ (%)	1.75	1.77	-
	n_{obs}	805	805	-
	n_{var}	43	43	-
	n_{powd}	0	9	0

* Comparable parameters from a multipole refinement including anisotropic extinction with the full non-averaged Ag data set of 8923 reflections; results of refinements comparable with those pursued in the present work were not reported by LSF (for details, see Lewis *et al.*, 1982).

extensive and least extinction-affected data sets be performed. In the following discussion, we compare the deformation density emerging from refinements with more extensive Ag : xtal and Ag : merge data sets with the recent *ab initio* results on $H_{20}Al_4O_5$ and $H_{18}Al_8O_{12}$ clusters reported by Brown & Spackman (1992) at the SCF level using mixed polarized basis sets.

Inclusion of the high-angle data that were excluded from the previous refinements should yield more reliable determinations of the electron distribution without the effects of thermal motion. The Ag $K\alpha$ data set was chosen for more detailed analysis for two reasons. Firstly, it is the most extensive, with 804 observations extending to a maximum $\sin\theta/\lambda$ of 1.495 Å^{-1}, and, secondly, although the $\sigma(I)/I$ ratio for the Ag : xtal data sets is on average three times larger than for the Mo : xtal data set (Lewis *et al.*, 1982), it is much less affected by extinction.

The results of the Hirshfeld model refinements with the complete Ag : xtal and Ag : merge data sets are given in Table 4, which also compares them with results reported by LSF (but it should be noted that the LSF results refer to a model that included anisotropic-extinction corrections and used the complete non-averaged data set). It can be seen that the positional and thermal parameters and the radial-function exponent values (with the exception of α_O) agree very well, giving some reassurance that the multipole-expansion equivalent of the Hirshfeld model yields results that are essentially identical. This confidence is strengthened when the LSF deformation density map in plane 1 (Fig. 1 in that work) is compared with the present multipole-expansion equivalent refinement (Fig. 8*a*) using the Ag : xtal data set and the same isotropic extinction model; the two maps are essentially identical, even at the nuclear sites (the lowest solid contour in the LSF maps appears to be the zero contour). This comparison establishes that the scale that was imposed on the data when $F(000)$ was calculated and included as an observation is indeed the same as that determined by LSF. The fit of the model to the data is once again improved for the merged data set, with ε dropping from 1203 to 1190 and the goodness of fit falling marginally, from 1.26 to 1.25, for the Ag : xtal and Ag : merge refinements, respectively.

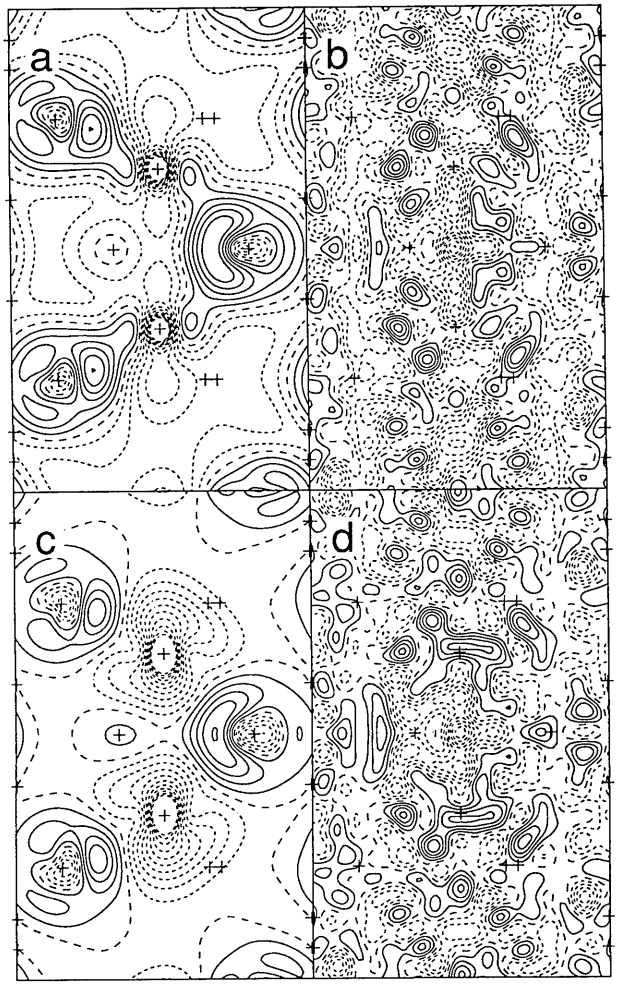

Fig. 8. (*a*), (*c*) Static multipole deformation density and (*b*), (*d*) residual Fourier maps in plane 1 obtained in multipole refinements with (*a*), (*b*) Ag : xtal and (*c*), (*d*) Ag : merge data sets. Contour interval 0.05 e Å^{-3}; full data refinement.

The major differences between the deformation density maps for the full-data refinements (Figs. 8 and 9) and for the restricted-data refinements (Figs. 2 and 3) are, as expected, in the vicinity of the nuclei. The deformation density in plane 1 for the Ag:xtal refinement (Fig. 8*a*) shows three positive lobes around the O atoms at the left of the map having peak maxima of 0.30 (4), 0.20 (4) and 0.17 (4) e $Å^{-3}$. The corresponding features for the Ag:merge map (Fig. 8*c*) have peak maxima of 0.24 (3), 0.14 (3) and 0.12 (3) e $Å^{-3}$, respectively, and those in the *ab initio* cluster maps are 0.25, 0.30–0.45 and 0.15–0.20 e $Å^{-3}$, respectively (Brown & Spackman, 1992). The elongated lobe of deformation density in the vicinity of the O atom at the right of the maps has a maximum of 0.29 (5) and 0.25 (3) e $Å^{-3}$ in the Ag:xtal and Ag:merge maps, respectively, in excellent agreement with the *ab initio* results of 0.25 e $Å^{-3}$ obtained for both clusters. These major features agree within two e.s.d.s for the two refinements, although, as noted for fits to the restricted data sets, the inclusion of the powder reflections systematically reduces the peak heights. In the vicinity of the Al nuclei, where the two maps differ most, there are two significant peaks of positive deformation density with maxima of 0.13 (3) and 0.12 (3) e $Å^{-3}$ in the Ag:xtal map, which are absent from the Ag:merge map. The corresponding points in the Ag:merge map have deformation density values of 0.00 (3) and −0.07 (3) e $Å^{-3}$, respectively, and no such features are observed in any of the *ab initio* cluster results.

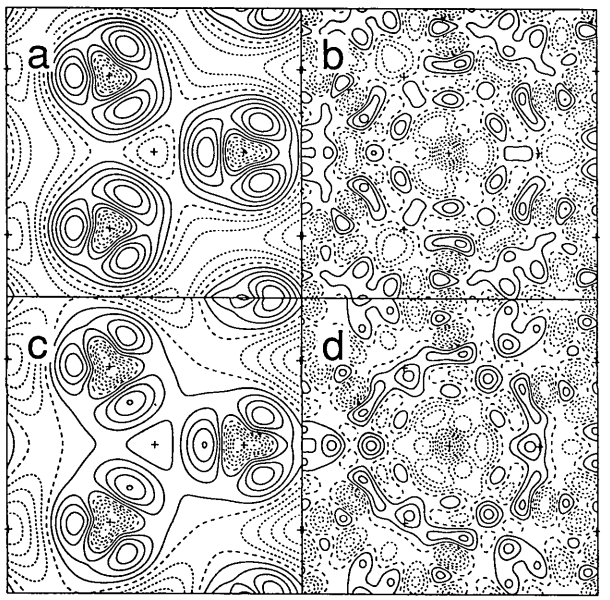

Fig. 9. (*a*), (*c*) Static multipole deformation density and (*b*), (*d*) residual Fourier maps in plane 2 obtained in multiple refinements with (*a*), (*b*) Ag:xtal and (*c*), (*d*) Ag:merge data sets. Contour interval 0.05 e $Å^{-3}$; full data refinement.

The deformation density in plane 2 for the Ag:xtal data set (Fig. 9*a*) shows three lobes of positive deformation density around each O atom, all with peak maxima of 0.29 (4) e $Å^{-3}$. The deformation density at the centre of the shared face is −0.09 (6) e $Å^{-3}$. The corresponding features in the Ag:merge map (Fig. 9*c*) are two lobes with peak maxima of 0.24 (3) e $Å^{-3}$ and one with a maximum of 0.25 (3) e $Å^{-3}$, and the centre of the shared face has a deformation density of 0.01 (3)e $Å^{-3}$. The features in these two maps again agree within two e.s.d.s and the Ag:merge results are again systematically lower than the Ag:xtal values and in better agreement with the *ab initio* cluster results (peaks of 0.25 e $Å^{-3}$ directed away from the shared face and 0.20 e $Å^{-3}$ in the shared face). There is now virtually quantitative agreement of both the Ag:merge and Ag:xtal results with the *ab initio* cluster results obtained by Brown & Spackman (1992). In particular, the Ag:merge results, being systematically lower than the Ag:xtal results, are generally in better agreement with the *ab initio* calculations.

Summary and concluding remarks

The results obtained in this work indicate that careful collection and reduction of powder diffraction data and application of the merging procedure described can successfully reduce the effects of extinction. One effect of the merging procedure for the Ag $K\alpha$ and Mo $K\alpha$ data sets was a marked improvement in the fit of the various pseudoatom models to the data, as evidenced by reductions in ε and the goodness-of-fit indices and the removal of systematic features from the residual Fourier maps.

It is also clear from this study that the quality of powder diffraction data that can be collected with currently existing techniques is sufficiently high to be used in accurate electron density analysis. Naturally, there are different problems associated with collecting and using powder data for this purpose, most notably with preferred orientation and closely or completely overlapping reflections but, with careful experimental technique and due regard for the way intensities are extracted from the raw data, reliable and reproducible structure factors can be obtained from powder diffraction data. This approach has several advantages, the most notable being the relative ease of powder-data collection (at least with conventional tube X-ray sources) and the large body of expertise that has developed in the collection of such data. The major limitation on the use of powder data in this way appears to be the problem of overlapping reflections: the larger the proportion of overlapping reflections present in the diffraction pattern, the less likely it is that the data will be amenable to accurate electron density analysis.

The differences between the deformation density maps for the Ag:xtal and Mo:xtal data sets are quite pronounced, particularly in the vicinity of the Al sites in plane 1 and the O sites in plane 2. The deformation density features emerging from the corresponding merged data sets are in somewhat better agreement, most noticeably so in plane 2 where significant positive deformation density in the shared octahedral face is observed. Complete agreement between the merged data results is not observed (or expected) since the effects of extinction in the two data sets, although relatively small in each case, are still different. While Ag:merge and Mo:merge require maximum extinction corrections of ~5%, the Mo:merge data set remains more seriously extinction affected in terms of the number of reflections requiring extinction corrections. For the purposes of conducting accurate electron density analyses, it is preferable to use the least extinction-affected data set possible. The Ag:xtal data set is the best currently available for corundum, and the success of the merging procedure in minimizing the effects of extinction seems to yield the most reliable experimental picture of the deformation electron distribution. Comparison of the results in Figs. 8(*c*) and 9(*c*) with recent *ab initio* cluster calculations supports these conclusions.

A University of New England Postgraduate Research Scholarship (to ASB), financial support from the Australian Research Council (to MAS) and a CSIRO-University of New England Collaborative Research Grant (to MAS and RJH) are gratefully acknowledged. ASB wishes to acknowledge the CSIRO Division of Mineral Products for generous provision of diffractometer and computing time for the collection and reduction of the powder data.

References

BECKER, P. (1977). *Acta Cryst.* A**33**, 243-249.
BECKER, P. J. & COPPENS, P. (1974). *Acta Cryst.* A**30**, 129-147, 148-153.
BRICOGNE, G. (1991). *Acta Cryst.* A**47**, 803-829.
BROWN, A. S. & SPACKMAN, M. A. (1992). *J. Phys. Chem.* **96**, 9200-9204.
CAUSA', M., DOVESI, R., ROETTI, C., KOTOMIN, E. & SAUNDERS, V. R. (1987). *Chem. Phys. Lett.* **140**, 120-123.
CLEMENTI, E. (1965). *IBM J. Res. Dev. Suppl.* **9**, 2.
COHEN, R. (1991). *Am. Mineral.* **76**, 733-742.
COPPENS, P. (1982). *Electron Distributions and the Chemical Bond*, edited by P. COPPENS & M. B. HALL, pp. 61-92. New York: Plenum.
DOLLASE, W. A. (1986). *J. Appl. Cryst.* **19**, 267-272.
GILMORE, C. J., HENDERSON, K. & BRICOGNE, G. (1991). *Acta Cryst.* A**47**, 830-841.
HILL, R. J. (1984). *Am. Mineral.* **69**, 937-942.
HILL, R. J. & HOWARD, C. J. (1986). Report No. M112. Australian Atomic Energy Commission, Sydney, Australia.
HILL, R. J. & MADSEN, I. C. (1991). *Z. Kristallogr.* **196**, 73-92.
HIRSHFELD, F. L. (1971). *Acta Cryst.* B**27**, 769-781.
HIRSHFELD, F. L. (1977). *Isr. J. Chem.* **16**, 226-229.
HOVESTREYDT, E. (1983). *Acta Cryst.* A**39**, 268-269.
International Tables for X-ray Crystallography (1974). Vol. IV. Birmingham: Kynoch Press. (Present distributor Kluwer Academic Publishers, Dordrecht.)
JANSEN, J., PESCHAR, R. & SCHENK, H. (1990). *Acta Cryst.* A**46**, C57.
JENKINS, R. (1989). *Reviews in Mineralogy*, Vol. 20. *Modern Powder Diffraction*, edited by D. L. BISH & J. E. POST, pp. 19-45. Washington, D.C: The Mineralogical Society of America.
KIRFEL, A. & EICHHORN, K. (1990). *Acta Cryst.* A**46**, 271-284.
KURKI-SUONIO, K. (1977). *Isr. J. Chem.* **16**, 132-136.
LEWIS, J., SCHWARZENBACH, D. & FLACK, H. D. (1982). *Acta Cryst.* A**38**, 733-739.
MCCUSKER, L. B. (1991). *Acta Cryst.* A**47**, 297-313.
MADSEN, I. C. & HILL, R. J. (1988). *J. Appl. Cryst.* **21**, 398-405.
PAWLEY, G. S. (1981). *J. Appl. Cryst.* **14**, 357-361.
PISANI, C., CAUSA', M., DOVESI, R. & ROETTI, C. (1987). *Prog. Surf. Sci.* **25**, 119-137.
RIETVELD, H. M. (1969). *J. Appl. Cryst.* **2**, 65-71.
SALASCO, L., DOVESI, R., ORLANDO, R., CAUSA', M. & SAUNDERS, V. R. (1991). *Mol. Phys.* **72**, 267-277.
SCHWARZENBACH, D. & LEWIS, J. (1982). *Electron Distributions and the Chemical Bond*, edited by P. COPPENS & M. B. HALL, pp. 413-430. New York: Plenum.
SCOTT, H. G. (1987). Program with Abstracts, IUCr Satellite Meeting on X-ray Powder Diffractometry, 20-23 August 1987, Fremantle, Western Australia. Abstract P28.
SCOTT, H. G. (1988). Personal communication to R. J. Hill.
SPACKMAN, M. A., HILL, R. J. & GIBBS, G. V. (1987). *Phys. Chem. Miner.* **14**, 139-150.
SPACKMAN, M. A. & STEWART, R. F. (1984). *Methods and Applications in Crystallographic Computing*, edited by S. R. HALL & T. ASHIDA, pp. 302-320. Oxford: Clarendon Press.
SPACKMAN, M. A. & WEBER, H.-P. (1988). *J. Phys. Chem.* **92**, 794-796.
STEWART, R. F. (1973). *J. Chem. Phys.* **58**, 1668-1676.
STEWART, R. F. (1976). *Acta Cryst.* A**32**, 565-574.
STEWART, R. F. & SPACKMAN, M. A. (1983). *VALRAY Users' Manual.* Chemistry Department, Carnegie-Mellon Univ., Pittsburgh, PA 15213, USA.
TSIRELSON, V. G., ANTIPIN, M. YU., GERR, R. F., OZEROV, R. P. & STRUCHKOV, YU. T. (1985). *Phys. Status Solidi A*, **87**, 425-433.
VINCENT, M. G., YVON, K. & ASHKENAZI, J. (1980). *Acta Cryst.* A**36**, 808-813.
VINCENT, M. G., YVON, K., GRÜTTNER, A. & ASHKENAZI, J. (1980). *Acta Cryst.* A**36**, 803-808.
WEBER, K. (1976). *Acta Cryst.* **23**, 720-725.
WILES, D. B. & YOUNG, R. A. (1981). *J. Appl. Cryst.* **14**, 149-151.
WILL, G. (1989). *Z. Kristallogr.* **188**, 169-186.